High resolution laser beam induced current focusing for photoactive surface characterization

C. Fernández-Lorenzo *, J.A. Poce-Fatou, R. Alcántara, J. Navas, J. Martín

Departamento de Química Física, Facultad de Ciencias, Universidad de Cádiz, Apartado de Correos 40, 11510 Puerto Real, Cádiz, Spain

Abstract

The micro-characterization of several surface properties of the solar cells can be accomplished using high-resolution laser beam induced current images. For obtaining these images, a very precise laser beam focusing on the photoactive surface is required. For this purpose, a methodology for obtaining the best focalization associated to the maximum of a peak curve has been developed. In this paper, a data set, obtained from the inner photoconversion properties of the system, has been evaluated with three different numerical analysis techniques: (a) derivative, (b) length and (c) Fourier Transform, in order to get the finest possible peak distribution. Then, an amount of 13 analytical peak curves using the Levenberg Marquardt algorithm to find the best curve that adjusts the data distribution have been analyzed.
© 2006 Elsevier B.V. All rights reserved.

1. Introduction

The study of solar cells using laser beam induced current (LBIC) technique – the measurement of the induced current when the surface is scanned with a laser beam – allows to evaluate its spatial conversion efficiency and also to detect possible irregularities due to the presence of impurities, processing heterogeneities, etc.

In order to obtain LBIC images with micrometric resolution and minimal geometric distortions, very little laser spot must be got, so, lenses with very short focal distance must be used [1–5]. Taking into account that these systems are of the order of a few micrometers in depth of field, the perfect positioning of the focal lens is of vital importance, since deviations of just a few micrometers in the optimum focusing position result in clearly unfocused images (Fig. 1).

Previous papers [6,7] have established the theoretical and experimental principles about the importance of using computational methods to determine the optimum distance of the focal lens positioning. This basic methodology uses the internal photoconversion properties of photosurface for optimizing the focusing process, analyzing the signal alterations generated by the presence of irregularities on the photoactive surface such as fingers, grain boundaries, dislocations, microdefects, etc. In this paper we are going to deepen in this study using three different numerical analysis techniques applicable to the data obtained by two different experimental methodologies and then fitting the resulting data to 13 mathematical peak functions. All the process has been performed in order to determining the most efficient focal technique methodology.

2. Focusing technique description

A TEM$_{00}$ mode laser beam presents a Gaussian irradiance distribution. This distribution is not modified by the focusing or reflecting of the beam by means of spherical optical elements and the irradiance is calculated by means of the expression:

$$I(r) = I_0 \exp\left(-\frac{2r^2}{w^2} \right), \qquad (1)$$

where r is the distance from the center of the optical axis and w the so-called Gaussian radius, defined as the distance from the

* Corresponding author. Tel.: +34 956 016 332; fax: +34 956 016 471.
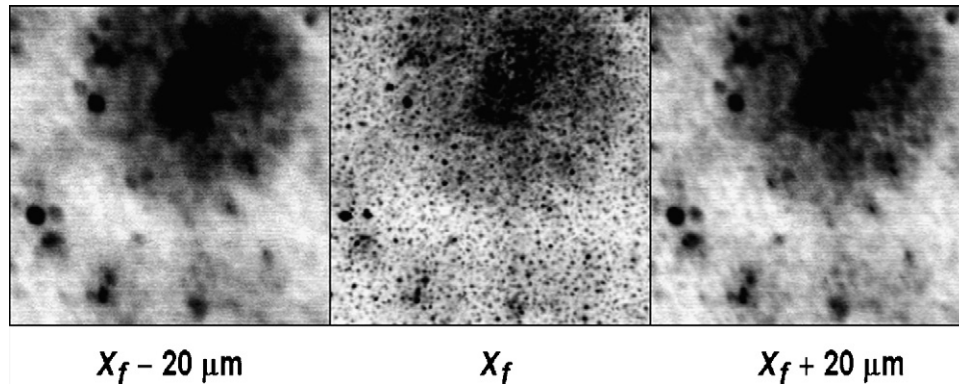E-mail address: concha.fernandez@uca.es (C. Fernández-Lorenzo).

Fig. 1. LBIC images of a microdefect in a monocrystaline solar cell (mc-Si), corresponding to a surface of 150 μm × 150 μm with a spatial resolution of 0.7 μm and a depth of focus of 6.52 μm. Notice the effect of the ±20 μm variation in the focal position in comparison with the optimum focusing distance, x_f.

optical axis to the position at which the intensity decreases to $1/e^2$ of the value on the optical axis.

When a monochromatic Gaussian beam is focused, the Gaussian radius in the area near the focus fits the equation:

$$w^2(x) = w_0^2 \left[1 + \left(\frac{\lambda x}{\pi n w_0^2} \right)^2 \right], \qquad (2)$$

where x is the coordinate along the propagation axis with the origin of coordinates being defined at the focal point, λ the wavelength value, n the refraction index of the medium and w_0 is the Gaussian radius value at the focus. The latter can be obtained from the expression:

$$w_0 = \left(\frac{2\lambda}{\pi} \right) \left(\frac{F}{D} \right), \qquad (3)$$

where F is the focal distance of the lens and D is the Gaussian diameter of the prefocused beam.

Another relevant magnitude is the depth of focus (DOF), defined (somewhat arbitrarily) as the distance between the values of x where the beam is $\sqrt{2}$ times larger than it is at the beam waist. This magnitude can be calculated from the expression:

$$\text{DOF} = \left(\frac{8\lambda}{\pi} \right) \left(\frac{F}{D} \right)^2, \qquad (4)$$

where the different magnitudes represent the same concepts we have previously defined. As it can be observed, the beam size at the focus and the depth of focus depend on the same factors, so that the smaller the former is, the smaller the latter will be, which in fact is going to determine some of the most relevant features of the system. That is why if we intend to have the maximum possible spatial resolution, it is necessary to be provided with an optimum focusing system given that the DOF value will also be very small; at the same time any non-essential optical elements that may contribute to the generation of distortions in the geometry of the beam must be avoided.

For a monochromatic beam, the energy irradiance is proportional to the photon irradiance. As we explained above, in an ideal focusing process, the beam power remains constant, which implies that the number of photons is also kept constant. Assuming that (a) only the photons adsorbed can generate electron–hole pairs according to a given quantum yield, (b) there are no biphotonic processes in normal conditions and (c) the power is low enough as to ignore thermal effects, then we can say that the intensity of the current supplied by the cell must be proportional to the density of incident photons and to the photoconversion efficiency of the cell. This implies that for an ideally homogeneous photoconversion surface, the current intensity generated will be independent of the focusing level, since, except when the size of the beam is larger than the active surface, the total number of photons will be a constant independent of its focusing level. In such a case the measure of current intensity would not be used to judge whether the laser beam is optimally focused.

The situation is quite different if the photoconversion surface has heterogeneities. In that case, the size of the heterogeneity would match the size of the photon beam. The definition of heterogeneity would depend on the type of cell we are working with. In monocrystalline solar cells we may consider the cell's edges or the electron-collecting conducting elements (fingers); in polycrystalline solar cells, in addition to the previously mentioned ones, we may also consider the grain boundaries, the dislocations or any other photoconversion defects and, in dye sensitized solar cells, porous semiconductors density irregularities, dye adsorption concentration, etc.

The electric current I_{SC} generated will depend on the illuminated surface quantum yield average value, which, at the same time is dependant of the spot size. This dependence can be used to optimally focus the laser beam on the active surface.

Prior to describe the focusing technique, the basic experimental set-up must be defined, that is shown in Fig. 2. According to this diagram, the solar cell or photoelectrical active surface is placed on the YZ plane. Normally to this surface and placed along the X-axis, a laser beam falls on. This laser is focused by a microscope objective lens, which can travel along that axis by means of a computer-controlled motorized stage. At the same time, the solar cell is fixed to two
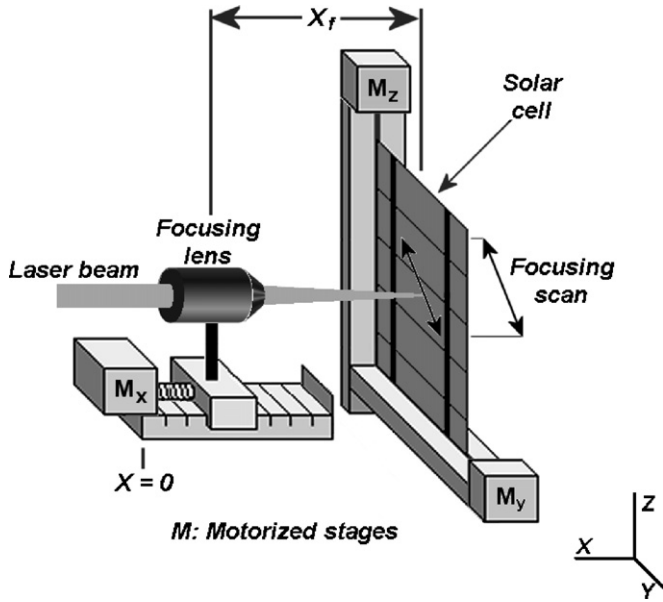
Fig. 2. Definition of coordinate axis and displacement directions of the photoactive surface and the focal lens.

motorized stages which allow it to move on the *YZ* plane, along a coordinate named ℓ so that

$$\Delta\ell = \sqrt{\Delta y^2 + \Delta z^2}, \qquad (5)$$

For every position along the ℓ coordinate, a value for the short circuit current is obtained (I_{SC}) that is proportional to its quantum efficiency. The graphic representation of $I_{SC}(\ell)$ versus ℓ gives rise to the so-called I_{SC}-curve.

In order to analyze the I_{SC}-curve, it is assumed that the photoactive surface is equivalent to an independent set of photoconversion units, each one having individual quantum efficiencies in the 0–100% range. These quantum efficiencies can be individually measured only if the size of the laser beam used as probe is equal or lesser than the aforementioned units. If the laser beam spot is greater than these basic units, the electric response obtained will be equivalent to the product of the quantum efficiency distribution values of the affected units multiplied by the laser beam geometry photonic intensity (monomodal Gaussian profile for the TEM_{00} mode).

Fig. 3a shows an example of an I_{SC}-curve. This one was obtained after performing a scan through a metallic current collector on a Silicon monocrystalline (mc-Si) solar cell. In this case, the laser beam has been focused by means of a 10× microscope objective lens, generating a minimum spot (w_0) on the order of 1.2 μm in diameter. Initially, the whole laser spot falls on a high photoconversion efficiency surface, generating a high I_{SC} value, showing small variations caused by little heterogeneities (zone 1), later, when the laser starts to intercept the finger, a gradual I_{SC} decreasing is generated (zone 2). If the collector width is greater than the laser spot diameter, the beam must travel through an area in which only a minimum current, associated to the diffuse light, is generated (zone 3). Subsequently the spot will gradually fall again on the photoactive sector (zone 4) until the spot again fully falls on the high efficiency photoactive surface (zone 5).

When the laser is not perfectly focused, the spot size diameter on the surface is larger than w_0 and the same scan through the metallic collector generates an I_{SC}-curve where signal measured at each position is a mean value of a wide zone. This generates a softer transition between regions with abrupt changes of their quantum efficiencies. In other words, the smaller the spot size, the more abrupt the I_{SC} transition between zones with different superficial photoactivity due to the different photoconversion units are better detected. Fig. 3b shows the aforementioned variations of the I_{SC}-curve according to the focal lens position. The I_{SC}-curve in the center of the figure corresponds to that one appearing in Fig. 3a, that is, the curve generated when the focal lens is in the optimum focusing position.

2.1. Scan methodologies

In order to obtain a data set with information about the optimum focusing position two experimental methodologies can be used. The first one, so called EM1, involves performing
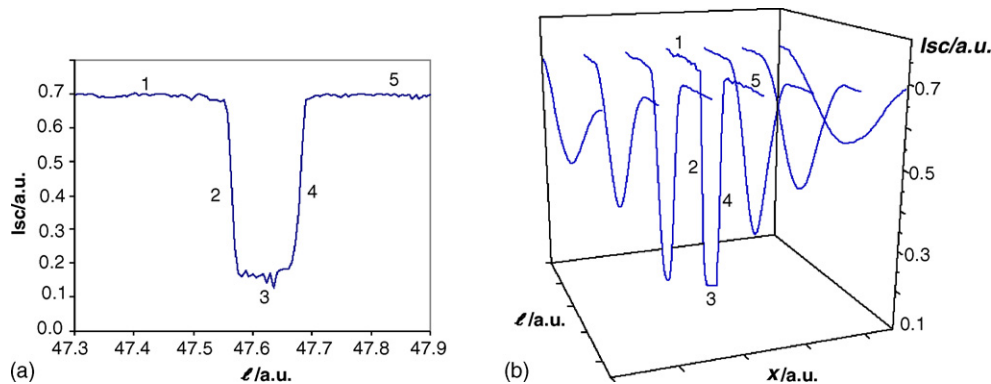

Fig. 3. (a) I_{SC}-curve obtained after performing a linear scan along a λ superficial coordinate on a Si(MC) solar cell and through a current collector. Three different types of zones can be distinguished: in zones 1 and 5 a full incidence of the laser beam on the active surface solar cell is produced; in zones 2 and 4 a partial intercept between the laser and the finger is attained; finally, in zone 3 the laser spot is fully intercepted by the finger. (b) I_{SC}-curve generated at different positions of the focal lens along *x*-axis.

successive linear scans along a ℓ coordinate on the photoactive surface, from different x_f focal lens positions. This methodology will lead us to an $EM1(I_\ell, x_f)$ data matrix, whose graphic representation by scan vectors is similar than the one shown in Fig. 3b.

The second methodology, called EM2, is a particular case of the first one and involves synchronizing the displacement along the ℓ coordinate with the focal lens displacement along the x coordinate. Then, only a vector data set is obtained and it is equivalent to the main diagonal of the aforementioned $EM1(I_\ell, x_f)$ data matrix, so a substantial reduction in the number of experimental points is achieved. In this case, the evaluation of the $EM2(x_f)$ data vector is carried out by defining several data subsets of n points of length, ranging from the first point to the total number of points minus n.

To analyze the previously defined data set, three numerical analysis techniques have been used, so called (a) derivative, (b) length and (c) Fourier Transform. The common purpose of all of them is to generate a new data set with a singular point associated to the optimum focusing position. This new data set is named *Focal-curve*. With this aim, the I_{SC}-curve data set properties must be numerically evaluated, under the optics of each methodology.

2.2. Derivative analysis

The transition slope between points with different quantum efficiency is defined as the values taken by the $dI_{SC}/d\ell$ derivative, which is related to the laser beam size. As it has been aforementioned, the smaller the spot size, the more abrupt the I_{SC} transition between points with a different superficial photoactivity and the larger the absolute value of $dI_{SC}/d\ell$. If the $d\ell$ is constant, then the derivative can be easily obtained as the dI_{SC}.

Fig. 4a shows the derivative of the I_{SC}-curve previously shown in Fig. 3a in a way that makes possible to recognize the above-mentioned one to five zones. Attention should be drawn to the fact that the absolute maximum values of the derivative are associated to transitions between photoconversion units with greater differential quantum efficiency. In our particular

case these maximum and minimum values are associated to the transition between the finger boundaries, so that only these transitions are significant. From this representation a new magnitude called Δ can be defined as the absolute difference between the maximum and minimum:

$$\Delta = \Delta_+ - \Delta_- = \max\left(\frac{dI_{SC}(\ell)}{d\ell}\right) - \min\left(\frac{dI_{SC}(\ell)}{d\ell}\right) \qquad (6)$$

At this point it is very easy to conclude that, the smaller the spot size (focused laser beam), the higher Δ value. Then, the representation of Δ according to the focal lens position, x, must result in a *Focal-curve* showing a peak distribution (Fig. 4b). In it, the optimum focusing position, x_f, corresponds to that one in which the value of Δ is the maximum.

2.3. Length analysis

This technique can be considered as complementary to the previous one and involves comparing the total length of the I_{SC}-curve for each focal lens position. As can be observed from Fig. 3b, the better the focused laser beam, the noisier I_{SC}-curve is obtained. This is a consequence to the better ability of the little laser spot to discern variations of quantum efficiency between small surface heterogeneities. In this case, the resulting I_{SC}-curve will be longer than the one obtained when the lens is positioned outside the focusing point.

The length of the I_{SC}-curve, L, may be calculated with the formula:

$$L = \sum_\ell (dI_{SC}(\ell)^2 + d\ell^2)^{1/2}. \qquad (7)$$

As in previous method, if the points through the ℓ coordinate are equispaced, then the $dI_{SC}/d\ell$ values are proportional to the values of the derivative in each point, and the length of the curve is equivalent to considering the derivative value addition for the total number of points. This is a fundamental difference regarding to derivative analysis because in this one only the most abrupt transition is significant.
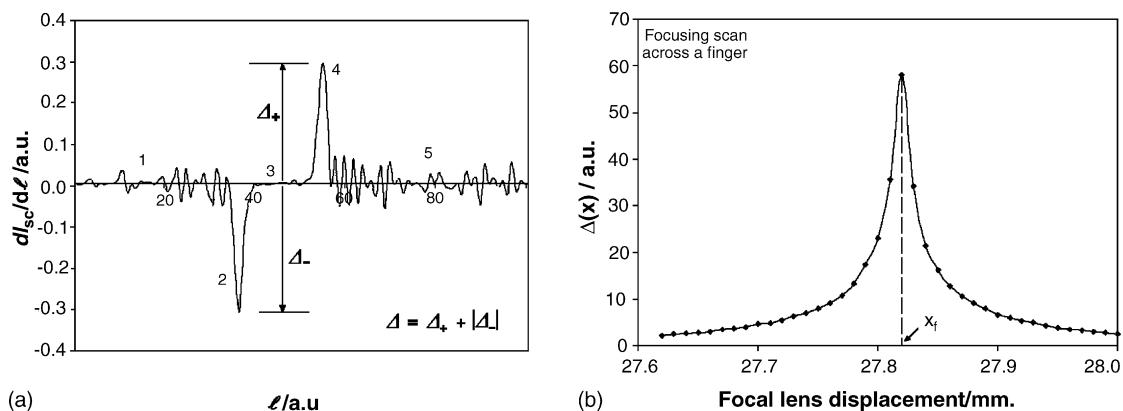

Fig. 4. (a) Numerical derivative of the I_{SC}-curve shown in Fig. 3a. Δ is the absolute maximum difference between $dI_{SC}/d\lambda$ values. (b) Representation of the Δ value versus positions of the focal lens. The optimum focusing position corresponds to the highest point reached by the curve.
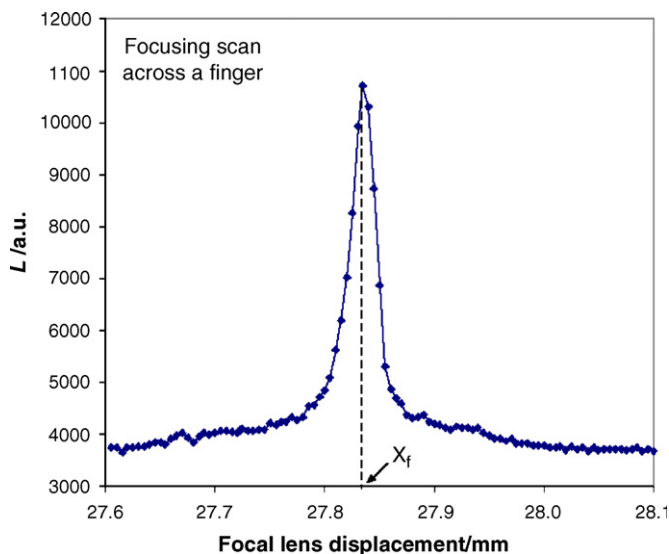
Fig. 5. Length *Focal-curve* representation of the data set shown in Fig. 3b. The optimum focusing position corresponds to the maximum point reached by the curve.

The representation of the curve length according to the *x* focal lens position leads to a new *Focal-curve* likewise with a peak distribution (Fig. 5). Newly, the *x* position in which the length is at its maximum value can be correlated with the optimum focusing position x_f.

Both analysis techniques cannot be applied to the EM2 scan methodology since *L* and *Δ* values obtained from each data subset should depend on the particular heterogeneities existing in the subset-scanned zone. Therefore, they cannot be compared with the values obtained from the subsequent data subsets that correspond to different superficial zones.

2.4. Fourier Transform analysis

Any function, periodic or not, can be represented by means of a superposition of periodic functions with different frequencies by applying the Fourier Transform. However, when one works with digital signals, there is a finite number of discrete values and therefore, it requires using discrete Fourier

Transform (DFT), a special case of the continuous Fourier Transform. In the one-dimensional discrete case, as our case, the discrete Fourier Transform is given:

$$F(u) = \frac{1}{N}\sum_{v=0}^{N-1} f(v)\ e^{-2\pi iuv/N} \quad \text{for } u = 0, 1, 2, \ldots, N-1.$$
(8)

In our case, $f(v)$ is the I_{SC}-*curve*, and v is the ℓ coordinate.

As stated before, a focused laser beam shows a higher resolution, which makes it possible to discern small signal variations that contribute significantly to the high frequency content of Fourier Transform (Fig. 6a). Therefore, the focusing distance is achieved, in the frequency domain, comparing a specific range of high frequency components in the I_{SC}-*curve* transform. Three consecutive steps must be applied to each I_{SC}-*curve*: (1) a Hanning window function, (2) an FFT function (the fast Fourier Transform is simply a DFT that is faster to calculate on a computer) and (3) a high pass filter or cut function that only leaves high frequencies.

The sum of high frequency amplitudes, Φ, can be represented versus the focal lens position leading to a new peak distribution curve (Fig. 6b). This analysis technique can be applied to any of the EM1 and EM2 experimental methodologies.

3. Treatment of the focal curve

The determination of the x_f position from the *Focal-curve* can be accomplished by numerical or algebraic methods. In both cases, several artifacts that habitually appear in the *Focal-curve* obtained as noise, asymmetric contour or multipeaks must be minimized. To diminish the associated noise to each scan point of the *Focal-curve*, to apply an accumulation method is the more appropriated way, either to individual points or to full scans. However, the other two artifacts do not show a clear dependence on known procedures. Normally, discerned or undiscerned multilevel photoactive structures can lead to obtain multipeaks and asymmetric contours, but other several circumstances can be cause of them. No particular dependence of these artifacts with the experimental methodology (EM1 or
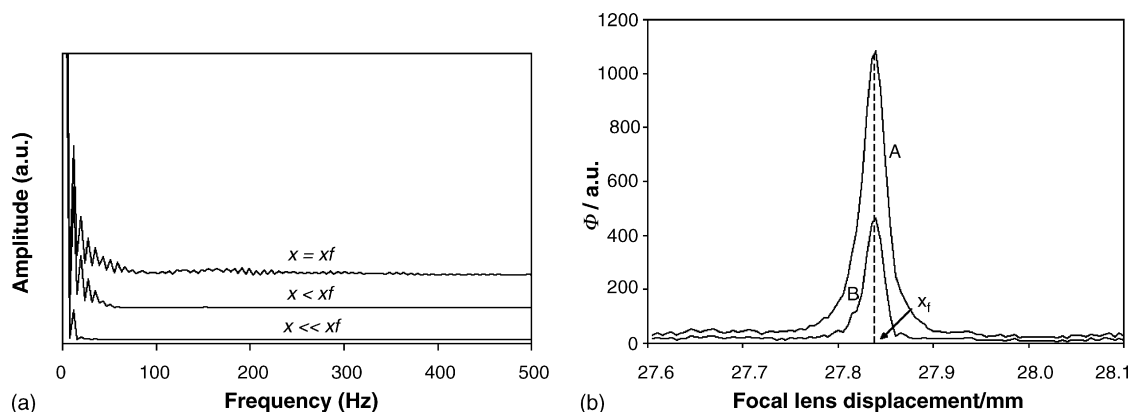

Fig. 6. (a) FFT of the signal proportional to the current in short-circuit, I_{SC}, in optimum focusing position and in prefocusing positions. (b) *Focal-curve* representation of the data set shown in Fig. 3b; curve A has been obtained using a high pass filter of 90% and curve B with a high pass filter of 60% in the frequency range.

Table 1
Functions used to analyze their ability of adjusting to the *Focal-curve* and accuracy of determine a precise focusing position

#	Function	Mathematical description	Parameters
F1	Gaussian	$V(x) = V_0 + \dfrac{S}{w}\sqrt{\dfrac{4\ln(2)}{\pi}}\exp\left[-4\ln(2)\dfrac{(x-x_f)^2}{w^2}\right]$	V_0, S, w, x_f
F2	Modified Gaussian	$V(x) = V_0 + S\exp\left[-\dfrac{1}{2}\left(\dfrac{|x-x_f|}{w}\right)^c\right]$	V_0, S, w, x_f
F3	Lorentz	$V(x) = V_0 + S\dfrac{2}{\pi}\dfrac{w}{4(x-x_f)^2 + w^2}$	V_0, S, w, x_f
F4	Voigt	$V(x) = V_0 + S\dfrac{2\ln(2)}{\pi^{3/2}}\dfrac{w_L}{w_G^2}\displaystyle\int_{-\infty}^{\infty}\dfrac{e^{-t^2}\,dt}{[\sqrt{\ln(2)}(w_L/w_G)]^2 + [\sqrt{4\ln(2)}((x-x_f)/w_G)-t]^2}$	V_0, S, w_G, w_L, x_f
F5	Pseudo Voigt	$V(x) = V_0 + V_m\left[\text{sf}\left(\dfrac{w}{(x-x_f)^2 + w^2}\right) + (1-\text{sf})\exp\left[-\dfrac{1}{2}\left(\dfrac{x-x_f}{w}\right)^2\right]\right]$	$V_0, V_m, \text{sf}, w, x_f$
F6	Type 1 Pseudo Voigt	$V(x) = V_0 + V_m\left[\text{sf}\dfrac{2}{\pi}\dfrac{w}{4(x-x_f)^2 + w^2} + (1-\text{sf})\dfrac{\sqrt{4\ln 2}}{\sqrt{\pi}w}\exp\left[-\dfrac{4\ln 2}{w^2}(x-x_f)^2\right]\right]$	$V_0, V_m, \text{sf}, w, x_f$
F7	Type 2 Pseudo Voigt	$V(x) = V_0 + V_m\left[\text{sf}\dfrac{2}{\pi}\dfrac{w_L}{4(x-x_f)^2 + w_L^2} + (1-\text{sf})\dfrac{\sqrt{4\ln 2}}{\sqrt{\pi}w_G}\exp\left[-\dfrac{4\ln 2}{w_G^2}(x-x_f)^2\right]\right]$	$V_0, V_m, \text{sf}, w_G, w_L, x_f$
F8	InvsPoly	$V(x) = V_0 + \dfrac{V_m}{1 + a_1\left(2\frac{x-x_f}{w}\right)^2 + a_2\left(2\frac{x-x_f}{w}\right)^4 + a_3\left(2\frac{x-x_f}{w}\right)^6}$	$V_0, V_m, a_1, a_2, a_3, x_f$
F9	Pearson VII	$V(x) = S\dfrac{2\sqrt{\text{sf}}\exp(\Gamma(2^{1/\text{sf}}-1))}{w\pi\exp(\Gamma(\text{sf}-1/2))}\left[1 + 4\dfrac{2^{1/\text{sf}}-1}{w^2}(x-x_f)^2\right]^{-\text{sf}}$	S, w, sf, x_f
F10	Log Normal	$\Delta(x) = \Delta_0 + \Delta_m\exp\left[-\dfrac{1}{2}\left(\dfrac{\ln(x)-\ln(x_f)}{w}\right)^2\right]$	V_0, V_m, w, x_f
F11	Asym2Sig	$V(x) = V_0 + V_m\dfrac{1}{1 + \exp[-((2(x-x_f)+w_1)/(2w_2))]}\left[1 - \dfrac{1}{1 + \exp[-((2(x-x_f)+w_1)/(2w_3))]}\right]$	$V_0, V_m, w_1, w_2, w_3, x_f$
F12	GCAS	$V(x) = V_0 + S\dfrac{\exp[-(1/2)((x-x_f)/w)^2]}{w\sqrt{2\pi}}\left[\dfrac{a_4}{24}\left(\dfrac{x-x_f}{w}\right)^4 + \left(\dfrac{a_3}{6}-\dfrac{a_4}{4}\right)\left(\dfrac{x-x_f}{w}\right)^3 - \dfrac{a_3}{2}\left(\dfrac{x-x_f}{w}\right) + \dfrac{a_4}{8} + 1\right]$	V_0, S, a_3, a_4, w, x_f
F13	Logistpk	$V(x) = V_0 + S\dfrac{4\exp(-(x-x_f)/w)}{(1 + \exp(-(x-x_f)/w))^2}$	V_0, S, w, x_f

The adjusting parameters have the next general significance: V_0 background level, V_m peak height, S area under the curve, w full width at half maximum, a_i general parameter, sf shape factor, x_f optimum focusing distance.

EM2) or with the analysis system (derivative, length or Fourier Transform) has been observed.

To apply the numerical method, it is enough to determine the focal lens position in which the peak distribution shows a maximum, and to associate that value with x_f. This is a very quickly methodology but shows significant errors and limitations due to the aforementioned artifacts. The maximum obtainable resolution with this method depends on the incremental value used in the focal lens positioning. A resolution improvement in one order of magnitude implies to measure a number of data two greater orders of magnitude. In the other side, the algebraic method involves adjusting a mathematical peak function to the *Focal-curve* and then determining x_f as the x value that maximizing the adjusted mathematical peak function. This methodology makes it possible mathematically to determine the maximum of the adjusted curve with as much precision as it is necessary.

In previous tests carried out by means of computerized simulation techniques it was demonstrated that a Pseudo-Voigt type 2 function is one of the peak functions that allows a better adjustment [6]. This function is a linear combination of the Gauss and the Lorentz distribution functions but establishing the same position parameter for both.

$$V(x) = V_0 + V_m\left[\text{sf}\,\dfrac{2}{\pi}\dfrac{w_L}{4(x-x_f)^2 + w_L^2} \right.$$
$$\left. + (1-\text{sf})\dfrac{\sqrt{4\ln 2}}{\sqrt{\pi}w_G}e^{-(4\ln 2/w_G^2)(x-x_f)^2}\right] \tag{9}$$

where $V(x)$ represents the values of Δ, L or Φ according to the position of the focal lens, w_L and w_G are the respectively FWHM values of the Lorentzian and Gaussian functions, V_m is the peak amplitude or height, sf is a proportionality factor, V_0
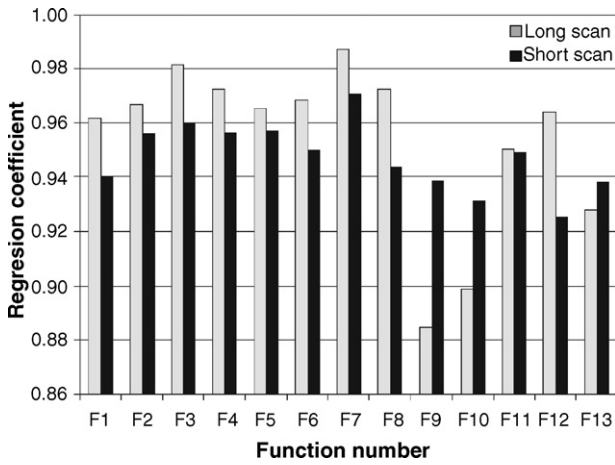
Fig. 7. Variation on R^2 average value for each type of function, for short and long scans.
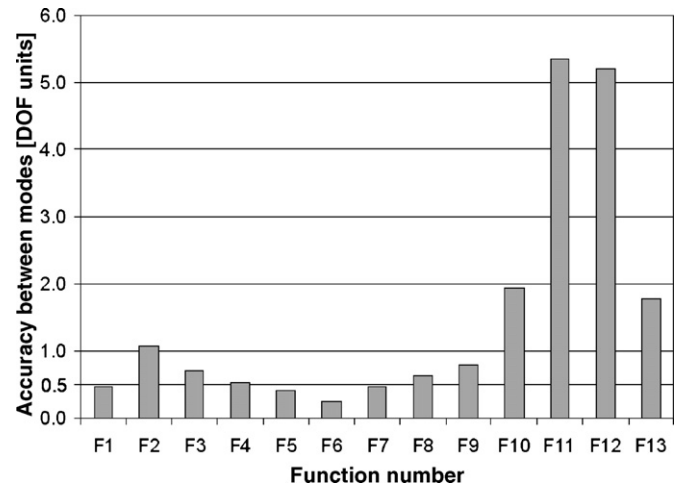

Fig. 9. Differences in the average calculated position for each type of function, for long scans with respect to short scans in DOF units.

is the displacement constant of the dependent variable and x_f is the curve maximum position.

However, we have observed that this function is suitable when the interval between the first and the last focal position analyzed is less than 1 mm. However, for bigger intervals, the *Focal-curve* shows a profile that, in several cases, is better defined by other peak functions. For this reason, it is necessary to carry out a comparative analysis of the several peak functions ability to fit to the *Focal-curve*.

Table 1 shows 13 peak mathematical functions that have been analyzed in order to check: (a) their ability to fit to the different experimental *Focal-curves* obtained through an LBIC system developed in our laboratory and (b) their ability to generate an accurate position. To carry out these objectives, it is necessary to work with real experimental data. For this reason, a polycrystalline Silicon solar cell, supplied by Isofotón S.A., has been used. This cell is a commercial one as used in popular consumption and it can be representative of a typical photosensitive systems. On this solar cell, LBIC scans on heterogeneities as fingers, crystal boundaries, microdefects, and monocrystal surfaces have been accomplished.

The fitting of the 13 functions with respect to the *Focal-curves* supplied for the different heterogeneities and for both short (a

±200 μm deviation) and long scans (a ±1 mm deviation), generates the set of R^2 values that is shown in Fig. 7. It may be observed that the best and most regular performances are obtained in the case of F1–F8 functions, whereas F9–F13 functions offer the worst fittings or the most important irregularities. On the other hand, the fittings to the long scans are usually better than to the short ones, although, according to the type of function, the former one generates greater fitting differences.

In the short scan series, the worst fitting values are provided by F12 (GCAS), F10 (Log Normal), F13 (Logistpk) and F9 (Pearson VII) functions and the three last ones also generate the worst fitting coefficients in the long scan series. By contrast, F7 (type 2 Pseudo Voigt) and F3 (Lorentz) functions provide the best fitting coefficients for both types of scan, although they are not very different regarding to the rest of the functions.

For the second parameter of ability, the objective is not easy to analyze since is not possible to determine how much exact is the focal position due to the own experimental characteristics (Fig. 8). It should be taken into account that little deficiencies concerning the perpendicularity of the laser with regard to the scan plane, together with surface deformities that are
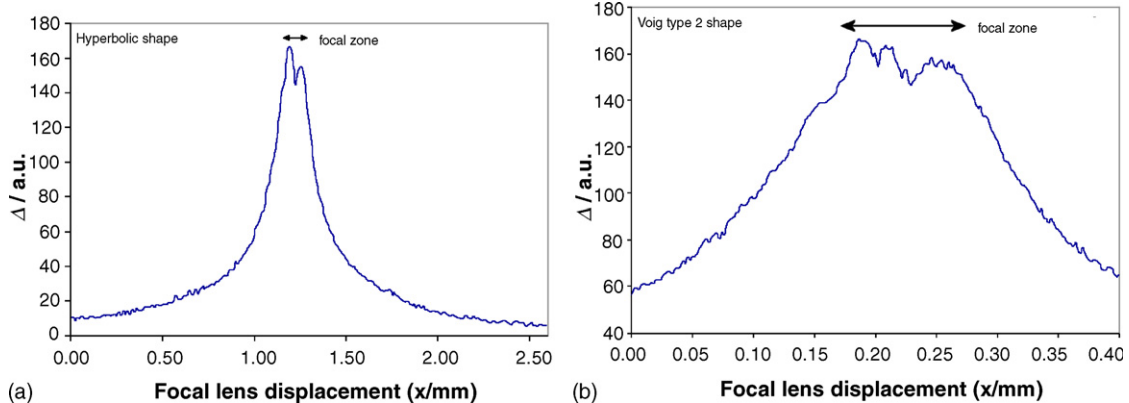

Fig. 8. Experimental *Focal-curve* showing an irregular peak profile for: (a) a long scan and (b) a short scan.

Table 2
Classification of the functions analyzed according to their ability to fit to the *Focal-curve* profile in long and short scans and to their ability to not generate focal distance discrepancies according to the type of scan

#	R^2		Focal distance discrepancy (DOF units)	Confidence index (%)
	Long scan	Short scan		
F1	0.96	0.94	0.47	23
F2	0.97	0.96	1.08	45
F3	0.98	0.96	0.70	65
F4	0.97	0.96	0.53	55
F5	0.97	0.96	0.42	53
F6	0.97	0.95	0.24	44
F7	0.99	0.97	0.48	95
F8	0.97	0.94	0.63	32
F9	0.88	0.94	0.79	0
F10	0.90	0.93	1.94	1
F11	0.95	0.95	5.34	0
F12	0.96	0.93	5.20	0
F13	0.93	0.94	1.78	8

characteristic of the manufacturing of solar cells, generate, in long scans, differences in the focal distance which are far greater than the accuracy of the method used.

The presence of multilevel structures in the microheterogeneity used as base of the focalization method is a new difficulty to be added to the aforementioned problems. Then, it is observed that the focal distance cannot be univocally defined, even in the most favorable case. For example, when a mc-Si solar cell is scanned, it must considered that the surface has a micropyramidal structure (chemically generated during the texturing process) and the photoactive surface shows an irregular profile of up to 15 μm from the apex to the base of these pyramids. In this case, although the scan is very short, the uncertainty in the focus value will be in the same order that the microstructural differences found on the surface.

The study of uncertainty in the focal distance, defined as the difference of the values for the long and short scans, is a possible way to analyze positioning data. If the adjusted function is accurate, the focal distance calculated from each scan method will must be identical or with minimal deviations, because this comparative dual analysis makes reference to the same point on the cell surface.

In order to refine this information, the data within the depth of focus (DOF) context can be analyzed. According to the focusing Gaussian beam theory, DOF is defined as the focal distance interval, around the focalization optimal point, in which the beam waist does not change more than 1.4 times of his value at focus. Any object placed into this interval will be focalized and therefore, any uncertainty in the determination of the focal distance lesser than DOF will not generate apparent defocusing in the object visualization. In our case, a lens, with a focal distance of 15.7 mm, a beam diameter of 7.8 mm and a wavelength of 632.8 nm, has been used, obtaining a DOF value of 6.52 μm, which means that, measuring from the focal point, only a ±3.26 μm displacement would be possible without having a noticeable loss of focusing.

Fig. 9 shows the different focal uncertainties generated for each type of function. It is possible to be seen again how F1–F9

functions generate the least differences between both types of scan (<7 μm), whereas F10–F13 functions are, on the contrary, the ones showing the worst performance, particularly F11 (Asym2Sig) and F12 (GCAS) functions where the reached values are in the range of 35 micrometers. In addition, only F1 (Gaussian), F5 (Pseudo Voigt), F6 (Pseudo Voigt type 1) and F7 (Pseudo Voigt type 2) functions generate a level of uncertainty at the focal position less than DOF/2.

In order to classify these functions, the values of R^2 and focal distance discrepancy have been normalized. The mean value of these normalized data is a confidence index about the ability of the considered function for fitting to the *Focal-curve* deduced from short and long scans and the ability for minimize the focal distance discrepancy between both scan modes (Table 2).

The application of these two approaches leads to the classification shown in Fig. 10. According to the score obtained, it is possible to confirm that only four functions have a confidence index greater than 50%. The Pseudo Voigt type 2 function provides the best results with a score of 95%, followed by the Lorentz function (65%) the Voigt function (55%) and the Pseudo
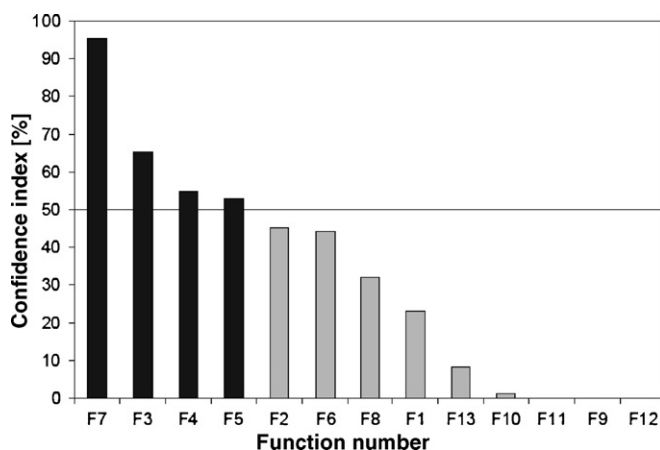

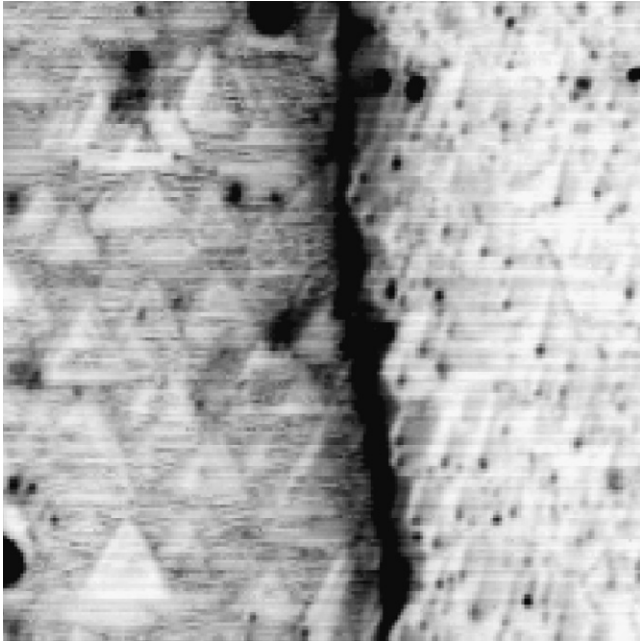Fig. 10. Confidence index representation obtained from normalized data of Table 2.

Fig. 11. LBIC image of a 215 μm × 215 μm surface of a polycrystalline silicon photovoltaic solar cell showing a grain boundary. The scan was performed at a resolution of 0.5 μm.

Voigt function (53%). The two last functions seem to have similar abilities to obtain a best R^2 and accurate on focusing distance.

4. Discussion and conclusions

Throughout this paper, two experimental methods (EM1 and EM2) for obtaining LBIC data from photoactive surfaces having information about focusing properties have been discussed under the optics of three different numerical analysis techniques (derivative, length and Fourier Transform). Each of them can be applied in order to obtain a peak *Focal-curve* where the optimum focal distance can be associated with the position of the maximum. This method makes possible to use the own photoconversion properties of the system to optimize the

focusing process and applying it to configure a high resolution LBIC system with a spatial resolution under 1 μm.

The *Focal-curve* generated from the aforementioned methods was also analyzed by adjusting to 13 mathematical peak functions in order to check their ability to fit to the experimental data and their ability to generate an accurate position x_f. The Pseudo Voigt type 2 function provides the best results with a confidence score of 95%, followed by the Lorentz function (65%).

The three analytical methods proposed generate similar performances for obtaining the optimum focusing distance, but their applicability is quite different depending on the type of photoactive surface. Thus, when zones with very different photoresponses are analyzed, as the microdefect shown in Fig. 1 and the grain boundary shown in Fig. 11, a good focal distance can be achieved by means of the derivative or length technique. In the last case (Fig. 11), it can clearly be observed how different crystal growth orientation presents different external photoconversion values, and that there is a sharp fall on the photoconversion value at the grain boundary, which is shown as a dark line. At the same time, it is possible to see in the left-hand side of the image that the texture of the wafer has pyramidal morphologies with a face orientation close to the image plane that we can see as triangular pattern.

A good general response is got, even when successive linear scans along a ℓ coordinate on the photoactive surface, from a few of x_f focal lens positions (gaps of the order of 20 μm in the displacement of the focal lens). In these conditions, the amount of manipulated data is small and it makes possible to obtain a good focusing in a short period of time.

However, in those cases in which the photoactive surface shows a great uniformity and only little heterogeneities can be found, the error in the position is lesser when the Fourier Transform technique is used. Fig. 12 shows the LBIC map generated according to the EM2 experimental methodology in (a) a dye-sensitized solar cell (DSSC), in which small signal variations can be noticed and (b) a monocrystalline silicon solar cell LBIC image. In this last case, the wafer texture has a micropyramidal structure with its symmetric axis perpendicular
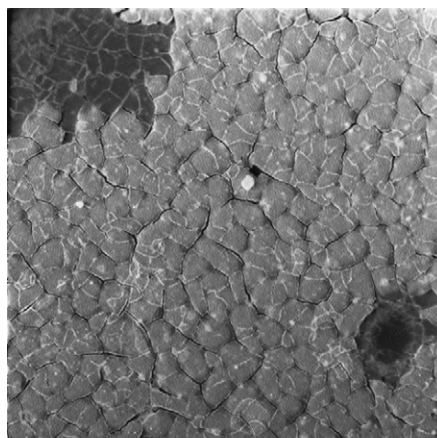
(a)
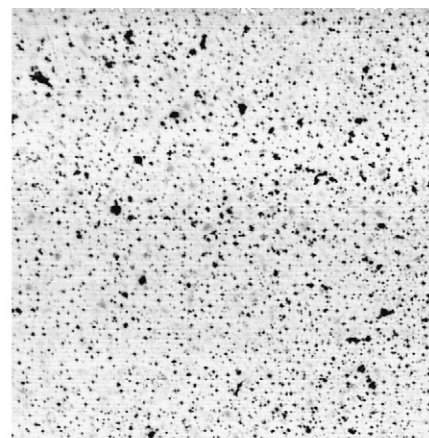
(b)

Fig. 12. LBIC image of (a) a 380 μm × 380 μm surface of a dye-sensitized solar cell and (b) a 500 μm × 500 μm surface of a monocrystalline silicon solar cell, performed at out a resolution of 1 μm.
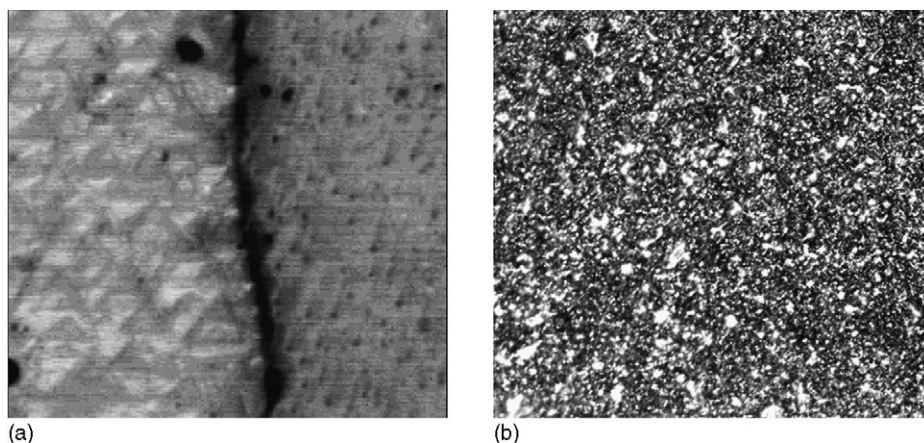
Fig. 13. Specular reflection image of: (a) a 215 μm × 215 μm surface of a polycrystalline silicon photovoltaic solar cell showing a grain boundary and (b) a 500 μm × 500 μm surface of a monocrystalline silicon solar cell. They belong with the respectively LBIC images of Figs. 11 and 12b.

to the wafer plane then its visual appreciation is azimuthal in the vertix-base plane direction. There are areas of low photoconversion corresponding to some of the peaks of these pyramids, possibly deriving from the breakage of such peaks. In this type of wafers the diffusion of phosphorus into the silicon crystalline structure is under 1 μm. The breakage of the pyramid apices due to mere friction, eliminates the semiconducting structure pn and no photoconversion can be obtained in these areas. In both cases the Fourier transform technique makes possible to achieve an adequate value of the focal distance.

This difference in applicability is due to the mathematical concept on which each technique is based. Whereas a derivative analysis is based on the search of the most abrupt transition between points with different superficial photoactivity, the Fourier Transform technique do not consider these abrupt transitions and proposes a more weight on the transitions generated by small heterogeneities.

On the other hand, the length analysis is an intermediate case of these two techniques. In the length analysis, both transitions (large photoresponse differences between points as well as the little heterogeneities), have a similar role to play. The length and the derivative analysis cannot be applied to EM2 experimental methodology on which a synchronous displacement between the superficial scan and the focal lens is performed. In this case, only the Fourier Transform technique can be applied.

Finally, this focusing technique allows setting up a system with the ability to obtain high resolution maps of the superficial variation of any photodependant property apart from the aforementioned induced current that can offer any material,

system or device. In Fig. 13, specular reflection images are shown and they belong with the respectively LBIC images of Figs. 11 and 12b. The laser beam focalization procedure used in this system is based on the fact that the photon beam sweeping on a photodependant and nonhomogeneous surface generates a variable response of the system according to the coupling between the photon beam size and the present heterogeneity size. Consequently, the detectable size of these ones depending on the illuminated surface that is minimum when the beam is perfectly focused.

Acknowledgements

References

[1] C.J.L. Moore, C.J. Miner, J. Cryst. Growth 103 (1990) 21.
[2] A.C. Ribes, S. Damaskinos, H.F. Tiedje, A.E. Dixon, D.E. Brodie, Sol. Energ. Mat. Sol. Cells 44 (1996) 439.
[3] M. Rinio, H.J. Möller, M. Werner, Solid State Phenom. 63/64 (1998) 115.
[4] C.A. Musca, D.A. Redfern, J.M. Dell, L. Faraone, Microelectron. J. 31 (2000) 537.
[5] F.J. Kao, J.C. Chen, S.C. Shih, A. Wei, S.L. Huang, T.S. Horng, P. Török, Opt. Commun. 211 (2002) 39.
[6] J.A. Poce-Fatou, J. Martín, R. Alcántara, C. Fernández-Lorenzo, Rev. Sci. Instrum. 73 (2002) 3895.
[7] J. Martín, C. Fernández-Lorenzo, J.A. Poce-Fatou, R. Alcántara, Prog. Photovolt: Res. Appl. 12 (2004) 283.